RESEARCH

Network analysis and experimental verification of Salvia miltiorrhiza Bunge-Reynoutria japonica Houtt. drug pair in the treatment of non-alcoholic fatty liver disease

Huafeng Chen[1,2†], Shengzhe Yan[1†], Qianru Xiang[4], Jiamin Liang[1], Xuejian Deng[1], Wanqin He[1], Yanzhen Cheng[1*] and Li Yang[1,3*]

Abstract

Context There are currently no approved specific clinical drugs for non-alcoholic fatty liver disease (NAFLD). Salvia miltiorrhiza Bunge-Reynoutria japonica Houtt. drug pair (SRDP) has been widely used in the treatment of chronic liver diseases. However, the mechanism of SRDP treating NAFLD remains unclear.

Objective Based on network analysis and in vitro experimental verification, we investigated the effect of SRDP on lipid deposition and explored its possible mechanism for the treatment of NAFLD.

Methods The TCMSP platform was used to screen the active metabolites of SRDP and corresponding targets. The GeneCards and OMIM databases were used to screen the NAFLD targets. The drug-disease intersecting targets were extracted to obtain the potential targets. Then the protein–protein interaction (PPI) and drug-active metabolites-target-disease network map was constructed. The DAVID database was performed to GO and KEGG pathway enrichment analysis for the intersecting targets. The core active metabolite and signaling pathway were verified by in vitro experiments.

Results Network analysis predicted 59 active metabolites and 89 targets of SRDP for the treatment of NAFLD. 112 signaling pathways were enriched for KEGG pathways, including PI3K-AKT signaling pathway,etc. It was confirmed that luteolin, the core active metabolite of SRDP, effectively reduced fat accumulation and intracellular triglyceride content in HepG2 fatty liver cell model. Luteolin could inhibit mTOR pathway by inhibiting PI3K-AKT signaling pathway phosphorylation, thereby activating autophagy to alleviate NAFLD.

†Huafeng Chen and Shengzhe Yan contributed equally to this work and share first authorship.

*Correspondence:
Yanzhen Cheng
chengyzx@163.com
Li Yang
yangli19762009@163.com
Full list of author information is available at the end of the article

Chen *et al. BMC Complementary Medicine and Therapies*   (2024) 24:305

Page 2 of 17

Discussion and conclusion The results of this study validate and predict the possible role of various active metabolites of SRDP in the treatment of NAFLD through multiple targets and signaling pathways. The core active metabolite of SRDP, luteolin can alleviate NAFLD by acting on the PI3K-AKT-mTOR signaling pathway to induce autophagy.

Keywords Salvia miltiorrhiza Bunge-Reynoutria japonica Houtt, Drug pair, Network analysis, Luteolin, PI3K-AKT-mTOR signaling pathway, Non-alcoholic fatty liver disease

Introduction

NAFLD is a clinicopathological syndrome mainly characterized by diffuse hepatocellular macrovesicular steatosis due to factors other than alcohol and other factors. Based on the extent of pathological changes and the presence or absence of inflammatory response and fibrosis, NAFLD can be classified as simple fatty liver (SFL) and nonalcoholic steatohepatitis (NASH), which can progress to liver fibrosis (LF), cirrhosis, and even hepatocellular carcinoma (HCC). According to the survey, the current global incidence of NAFLD is about 6.3–45%, and this prevalence is increasing annually [1]. In Western countries, NAFLD has gradually become the main cause of chronic liver diseases. In China, the prevalence of NAFLD has surpassed chronic viral hepatitis as the leading cause of chronic liver disease [2].

There are currently no drugs or procedures approved to treat NAFLD. Lifestyle changes remain the cornerstone approach to its management [3]. The multi-factor and heterogeneity of NAFLD indicates that it cannot be managed as a single disease or effectively treated with a single therapeutic agent. Chinese medicine, with its numerous bioactive metabolites, multiple therapeutic principles, and low adverse drug reactions, is playing an increasingly important role in the treatment of NAFLD [4].

Salvia miltiorrhiza Bunge [Lamiaceae; Salviae miltiorrhizae radix et rhizoma] (Named Danshen in Traditional Chinese Medicine) has been extensively used to treat metabolic syndromes such as hypertension, dyslipidemia, and hyperglycemia by acting on hyperlipidemia and visceral lipids to reverse the metabolic syndrome [5]. Growing evidence suggests that Salvia miltiorrhiza Bunge may have a positive effect on NAFLD [6] and is associated with a reduced risk of metabolic disorders in preclinical and clinical trials [6–8]. In a randomized controlled trial involving 800 NAFLD patients across eight trials, Salvia miltiorrhiza Bunge was found to alleviate hepatic lipid degeneration by reducing plasma levels of transaminases [7]. Reynoutria japonica Houtt. [Polygonaceae,Polygoni Cuspidati Rhizoma et Radix] (Named Huzhang in Traditional Chinese Medicine), another Chinese botanical drug, exhibits various pharmacological activities such as anti-inflammatory, antioxidant, metabolic modulation, microcirculation improvement, hepatoprotection,

and immunity enhancement [9]. In recent years, a large number of studies [10–12] have demonstrated that the active metabolites of Reynoutria japonica Houtt. can exert therapeutic effects on NAFLD by improving insulin resistance, reducing oxidative stress, regulating lipid metabolism, improving endoplasmic reticulum stress, and reducing inflammatory infiltration. When summarizing the experience of using traditional Chinese medicines for the prevention and treatment of liver diseases, Salvia miltiorrhiza Bunge and Reynoutria japonica Houtt. are frequently used in combination as classical pair for the treatment of liver diseases due to their good therapeutic effects [13, 14]. However, due to their complex composition, and diverse mechanisms, further research and promotion of clinical application about them are not facilitated.

This computer-based network analysis method, which combines systems biology, multidirectional pharmacology, and technologies such as histology, and high-throughput sequencing, can reveal the complex relationship network among drugs, diseases, active metabolites, and targets. This approach can reveal the mechanism of Chinese medicine for the treatment of diseases in a more comprehensive manner. Therefore, this study utilized network analysis and experimental validation to investigate the mechanism of SRDP in treatment of NAFLD. The core active metabolite, luteolin, and the key signal pathway PI3K-AKT-mTOR were selected for experimental verification. Luteolin was found to inhibit mTOR phosphorylation by regulating PI3K-AKT pathway, thereby inducing autophagy to alleviate NAFLD. SC79, an activator of AKT phosphorylation, was used to further confirmed the role of luteolin in this pathway. This study comprehensively revealed the active metabolites, specific targets, and mechanisms of SRDP in treating NAFLD, providing a theoretical basis for studying the clinical application of SRDP in NAFLD.

Materials and methods

Screening of active metabolites and targets acquisition of SRDP

The active metabolites of Salvia miltiorrhiza Bunge and Reynoutria japonica Houtt. were obtained from the Traditional Chinese Medicine System Pharmacology Database

and Analysis Platform (TCMSP) (https://www.tcmsp-e.com/#/home) [15]. The screening conditions were set as oral bioavailability (OB) ≥ 30% and drug similarity (DL) ≥ 0.18. The targets of relevant active metabolites were also obtained in the TCMSP database. Predicted target protein names were converted to the corresponding human-derived gene names by Uniprot database (http://www.uniprot.org/) [16].

Screening of NAFLD related targets

The genes related to NAFLD were searched by entering the keyword "non-alcoholic fatty liver disease" in the GeneCards database (http://www.genecards.org/) [17] and OMIM database (http://www.ncbi.nlm.nih.gov/omim) [18]. Duplicate genes obtained in GeneCard and OMIM were removed and the remaining genes were matched with the drug targets to obtain the potential targets of SRDP for the treatment of NAFLD.

Construction of drug-active metabolite-target-disease network

Active metabolites and potential targets were visualized and analyzed using Cytoscape 3.7.1 software [19] to draw the drug-active metabolite-target-disease network. CytoNCA was used to cluster Betweenness Centrality and Closeness Centrality.

Construction and analysis of protein–protein interaction (PPI) network

The intersecting target proteins were entered into the String database (https://string-db.org/cgi/input.pl) [20] to obtain PPI networks. The results were imported into Cytoscape 3.7.1 software, and then the topological properties of the network were analyzed using the "Network Analysis" function. The key target proteins were obtained by setting two times the median Degree value as the threshold (Cluster Maker plug-in).

Gene Ontology (GO) enrichment analysis and Kyoto Encyclopedia of Genes and Genomes (KEGG) enrichment analysis

The intersecting target proteins were entered into the String database the DAVID database (https://david.ncifcrf.gov/) [21]. The restricted species was "Homo sapiens". The GO and KEGG enrichment analysis of potential targets of SRDP for NAFLD treatment was performed by "Functional Annotation". $p < 0.05$ was considered statistically significant. The results were visualized by bioinformatics online tool (http://www.bioinformatics.com.cn/) and Cytoscape 3.7.1 software.

Molecular docking validation

Based on the above analysis and literature review, key active ingredients were selected for molecular docking with key targets. AutoDockvina software was used to pretreat the target protein, and introduce the small-molecule ligands. Subsequently, the target protein and the small-molecule ligands were converted into pdbqt files and subjected to molecular docking to obtain the minimum binding energy required for docking. PyMOL software was used to visualize the results.

In vitro experimental validation
Cells and reagents

The human hepatocellular carcinoma cell line (HepG2) was donated by the Department of Pathology, School of Basic Medical Sciences, Southern Medical University and purchased from the Shanghai Institute of Cell Biology, Chinese Academy of Sciences. Luteolin was from Macklin (Shanghai, China). Palmitic acid sodium (PA) was from Inno-Chem Science & Technology Co., Ltd. (Beijing, China). SC79 was from Beyotime (Shanghai, China). Bovine serum albumin (BSA) was from Procell Life Science&Technology Co.,Ltd. (Wuhan, China). 0.25% trypsin solution and Dulbecco's modified medium were from NCM Biotech (Suzhou, China). All other chemicals and reagents were purchased commercially and are of analytical grade.

Mouse anti-PI3-kinase p85α (phospho Tyr607) Antibody and mouse anti-PI3-kinase p85α antibody were from Taizhou Baijia Biotechnology Co., Ltd. (China). Rabbit anti-AKT antibody, rabbit anti-p-AKT antibody, rabbit anti-mTOR Antibody, Rabbit anti-Phospho-mTOR (S2448) antibody, rabbit anti-SQSTM1/p62 antibody, rabbit anti- LC3B antibody, mouse anti-GAPDH antibody, goat anti-mouse IgG Alexa Fluor 594, goat anti-mouse IgG Alexa Fluor 488 and goat anti-Rabbit Mouse IgG-HRP were from Abmart Shanghai Co.,Ltd. (Shanghai, China).

Solution preparation

Preparation of PA molding solution: 11.13 mg of PA was weighed in 1 mL of deionized water and dissolved in water bath at 75℃. 0.3 g of BSA was weighed and dissolved in PBS in a 55℃ water bath to prepare a 30% solution of BSA. PA solution was immediately mixed with 30% BSA solution to produce 20 mmol/L PA stock solution, filtered through a 0.22 μm microporous membrane for sterilization, and stored at − 20℃ in the dark.

Preparation of Luteolin solution: 10 mg was dissolved in 698.7 μL DMSO to produce 50 mmol/L mother solution, which was sterilized by filtration through a 0.22 μm microporous membrane and stored at 4℃ in the dark.

Chen *et al. BMC Complementary Medicine and Therapies*   (2024) 24:305

Page 4 of 17

Cell culture, construction of NAFLD model in vitro and experimental grouping

HepG2 cells were cultured in DMEM medium containing 10% fetal bovine serum (containing 1% penicillin and streptomycin) in an incubator at 37℃, 5% CO2, 95% humidity. The cells at logarithmic growth stage were taken for the experiments. HepG2 cells were placed in a hepatocyte steatosis model containing 0.4 mM PA induced for 24 h. HepG2 cells were grouped according to whether they were treated with PA, luteolin, and SC79.

Cell activity assay

100 µL cell suspension (approximately 5000 cells/well) was inoculated into each well of the 96-well plate. The plates were pre-cultured in a humidified incubator for 12 h to allow the cells to adhere. According to the previous research foundation of our research group, then the medium was changed to DMEM supplemented with 0 mM (control), 0.2 mM, 0.4 mM, 0.6 mM, 0.8 mM, 1.0 mM PA working solution and incubated for 12, 24, 48 h. Five replicate wells were set for each group. Under light-proof conditions, 10 µL CCK-8 reagent and 90 µL DMEM were added to each well and then incubated for 2 h. The absorbance values were analyzed at 450 nm using an enzyme marker (Thermo Fisher Scientific). Absorbance values were analyzed with a microplate reader (Thermo Fisher Scientific) at a wavelength of 450 nm. The absorbance values of HepG2 cells treated with 0 mM, 5 mM, 10 mM, 20 mM, 40 mM, 80 mM, 160 mM luteolin working solution were determined in the same way based on the above obtained PA intervention concentrations. Based on the PA and luteolin intervention concentrations obtained above, the absorbance values after treatment of HepG2 cells with 0 µM (control), 2.5 µM, 5.0 µM, 7.5 µM, 10.0 µM, 20.0 µM SC79 working solution were determined.

Modified Oil Red O staining

The modified oil red O staining kit was purchased from Beyotime Biotechnology (Shanghai, China). After washed once with PBS according to the instructions, the cells were covered with the washing solution for 20 s, and a proper amount of modified oil red O staining solution was added for staining for 10–20 min. At the end of the staining, a proper amount of staining washing solution was added, allowed to stand for 30 s, and then washed with PBS for 20 s. The cells were uniformly covered with an appropriate amount of PBS and observed and photographed under a bright-field scanning microscope (LEICA, Germany) at a magnification of 100 or 400 times.

Measurement of triglyceride content

To quantify intracellular lipid accumulation, the triglyceride (TG) content of HepG2 cells was measured using the Tissue Cell Triglyceride Enzyme Assay Kit (ApplyGen Technology, Beijing, China) according to the reagent instructions.

Western blotting to detect changes in the expression of PI3K-AKT-mTOR signaling pathway and autophagy-related protein levels in each group of cells

Cell culture interventions were performed in 6-well plates. The cells were lysed according to the ratio of RIPA: protease inhibitor: phosphate inhibitor=100:1:1. The protein concentration of lysates was quantified using the BCA protein assay kit. The protein supernatants were mixed with $5 \times$ loading buffer and then placed in a metal bath at 95–100 C for 10 min. Samples were added, subjected to run-time electrophoresis (90 V 30 min, 120 V 1 h), membrane transfer (200 mA 1.5 h or 3 h). PVDF membrane was blocked by shaking at room temperature for 1 h. The primary antibody was added into a refrigerator at 4 C for incubation overnight. The membrane was washed three times with TBST, and incubated with shaking table and secondary antibody for 1 h at room temperature. The membrane was washed three times again with TBST. Chemiluminescent solution (solution A: solution B=1: 1) was added into PVDF membrane for imaging using Multifunctional molecular imaging system (Alliance Q9). Optical density analysis of the protein bands was performed by ImageJ software, using the GAPDH protein as an internal control.

Statistical analysis

The results are represented as mean±SEM. GraphPad Prism 8.0 was used for statistical significance analysis and visualization. T-test was used for comparison between the two groups, and one-way analysis of variance was used for comparison between multiple groups. Statistical significance was defined as $p < 0.05$.

Results

Screening of active metabolites of SRDP

The TCMSP platform retrieved a total of 65 potential active metabolites of Salvia miltiorrhiza Bunge, 10 potential active metabolites of Reynoutria japonica Houtt. (Supplementary Table), and one common active metabolite, namely luteolin. 58 active metabolite-related targets of Salvia miltiorrhiza Bunge and 92 active metabolite-related targets of Reynoutria japonica Houtt. were obtained.

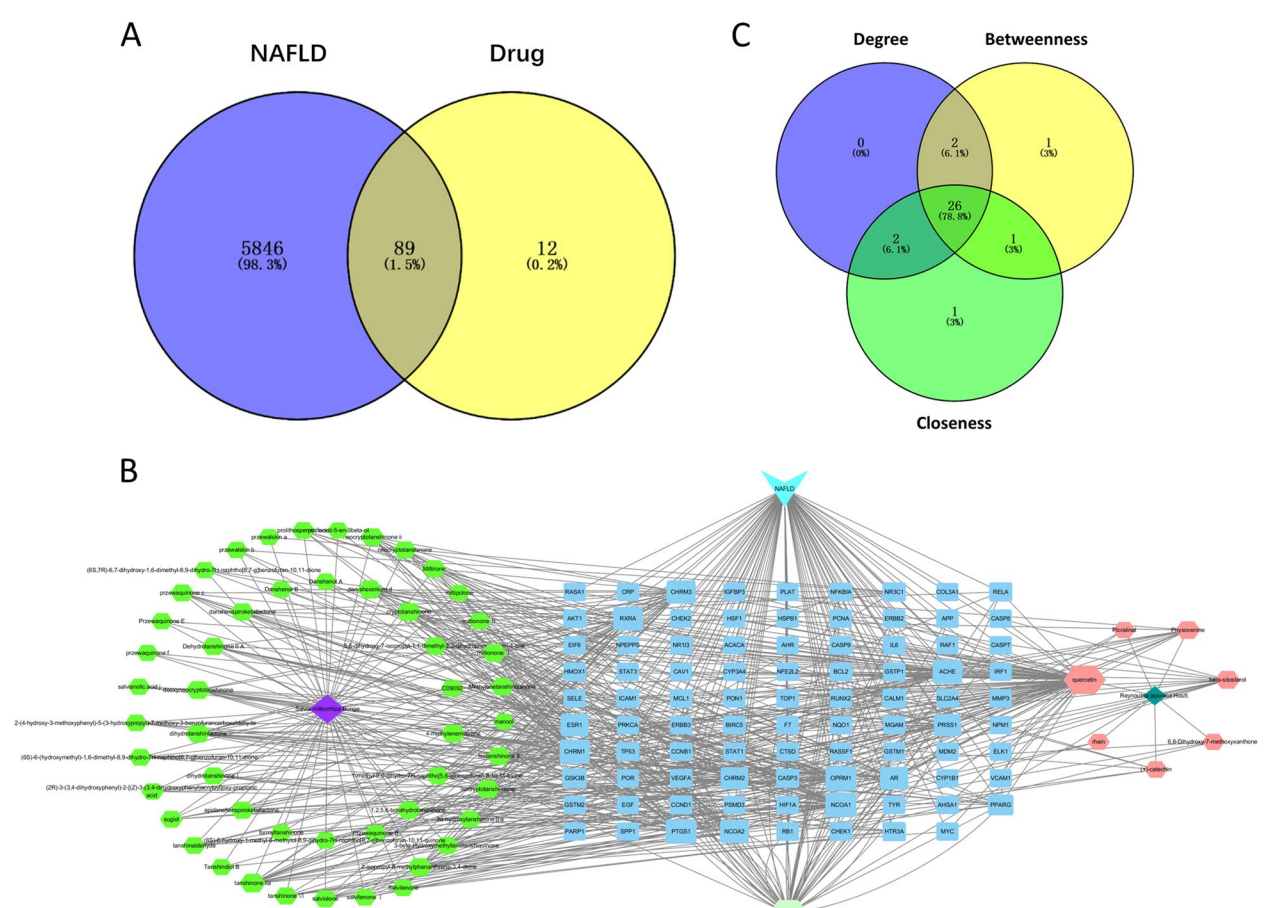**Drug-active metabolite-target-disease network diagram**

5520 disease-related genes were obtained from GeneCard databases, and 529 disease-related genes were obtained from OMIM databases. After eliminating repeated targets, 5935 disease-related targets were obtained. 89 targets were obtained by crossing the disease-related targets and active metabolite-related targets (Fig. 1A). 59 active metabolites acting on the intersecting targets were identified. The active metabolite-target-disease network diagram was drawn by Cytoscape3.7.1 software (Fig. 1B). The network consisted of 151 nodes and 632 edges. The size of each node graph was proportional to its Degree value.

The top 30 active metabolites of Cytoscape network topology parameters, including Degree, Betweenness Centrality and Closeness Centrality, were selected to draw a Venn diagram, resulting in 26 intersections (Fig. 1C).

The top three active metabolites were quercetin (Degree: 72.0, Betweenness: 4385.217, Closeness: 0.5928854), luteolin (Degree: 60.0, Betweenness: 2096.1836, Closeness: 0.45592704), and tanshinone IIA (Degree: 17.0, Betweenness: 381.80765, Closeness: 0.41551247), in which luteolin is the core active metabolite shared by Salvia miltiorrhiza Bunge and Reynoutria japonica Houtt.

PPI network analysis results

After removing 2 discrete nodes, the PPI network contained 87 nodes and 991 edges (Fig. 2). The nodes represent target proteins, each edge represents the interaction between target proteins, and the thickness of the edge represents the strength of the interaction force. The 15 main targets were selected to build the PPI sub-network (Fig. 2), which showed that AKT1, TP53, MYC, ESR1, and CASP3 were most closely connected.

Fig. 1 Potential action targets of SRDP and drug-active metabolite-target-disease network diagram. **A** Venn diagram of the SRDP and NAFLD target. **B** Interaction network diagram between Chinese drugs, active metabolites, potential targets and diseases. The prisms represent drugs, hexagons represent active metabolites, V-shape represents NAFLD, rectangles represent potential action targets, lines represent the interactions between the nodes, purple prisms represent Salvia miltiorrhiza Bunge, dark green prisms represent Reynoutria japonica Houtt, green hexagons represent active metabolites corresponding to Reynoutria japonica Houtt, red hexagons represent active metabolites corresponding to Salvia miltiorrhiza Bunge, light green hexagons represent luteolin, the active metabolite shared by SRDP. **C** Degrees, Betweenness Centrality and Closeness Centrality of Top 30 active substances Venn diagram

Chen *et al. BMC Complementary Medicine and Therapies*   (2024) 24:305

Page 6 of 17
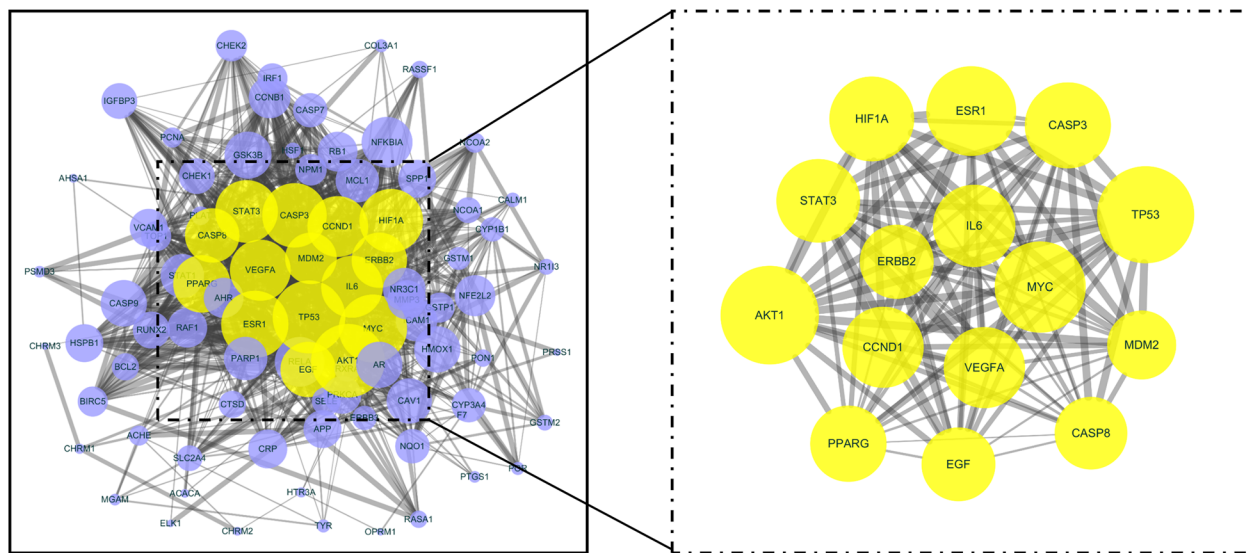
Fig. 2 PPI network analysis results. The left graph shows the potential target protein interaction network, and the right graph shows the key target protein sub-network

Results of GO enrichment analysis and KEGG pathway analysis

The results of GO enrichment analysis showed that a total of 85 entries were enriched for molecular functions, 335 entries were enriched for biological processes, and 50 entries were enriched for cellular components. The top 10 entries were plotted as bar graphs according to the number of enriched genes (Fig. 3A). A total of 112 signaling pathways were enriched using DAVID database, including PI3K-AKT, AGE-RAGE, MAPK, HIF-1, and p53 signaling pathway. The top 20 entries were plotted as bar graphs according to the number of enriched genes (Fig. 3B).

Molecular docking

Combining the degree value of protein interactions of key targets in PPI network analysis, the network degree analysis of "drug-active ingredient-target-disease network", and literature review, the core active ingredients, quercetin, luteolin, tanshinone iia, beta-sitosterol, cryptotanshinone, and cryptotanshinone, were selected to dock with the key target proteins AKT1, TP53, MYC, ESR1, and CASP3. The molecular docking results showed that the binding energy of these active ingredients docked with key target proteins was less than -5 kcal/mol (Table 1, Fig. 4F). The binding energy was negative, which showed that the binding effect of them was good. The docking results of luteolin, the core ingredient with the high Degree value and shared by DHHP, with AKT1, TP53, MYC, ESR1 and CASP3 were visualized using PyMOL software (Fig. 4A-E).

Effect of different concentrations of PA and luteolin on HepG2 cell activity and triglyceride content

The cell inhibition rate curves were plotted (Fig. 5A), and the IC50 values of cell inhibition rate of PA intervention for 12, 24, and 48 h were calculated by regression equation as 0.7251, 0.6894, and 0.5176 mM, respectively. Intracellular TG content of HepG2 cells was higher than that of the control group after different concentrations of PA treatment ($P < 0.05$). The intracellular TG content in 0.4 mM, 0.6 mM, 0.8 mM, and 1.0 mM PA group were higher than that of the control group ($P < 0. 001$). The intracellular TG content increased with the increase in PA concentration, but there was no significant difference in TG content between the 0.4 mM PA, 0.6 mM PA, 0.8 mM PA, and 1.0 mM PA groups (Fig. 5B). Combined with the above results of inhibition rate and triglyceride content analysis after PA intervention, the intervention concentration and time of PA were formulated as 0.4 mM and 24 h.

After 48 h of luteolin intervention, the cell inhibition rates of different concentration groups were higher than 50%. The IC50 values of cell inhibition rates at 12 and 24 h of luteolin intervention were 57.88 and 36.48 mM, respectively, calculated by regression equation (Fig. 5C). Under 0.4 mM PA condition, the TG content of 20 mM, 40 mM, and 80 mM luteolin group decreased significantly compared with PA group ($P < 0.001$), and the TG content was not statistically different compared with blank control group (Fig. 5D). Combined with the above analysis, the intervention concentration and time of luteolin were formulated as 20 mM and 24 h.

Chen *et al. BMC Complementary Medicine and Therapies*   (2024) 24:305

Page 7 of 17
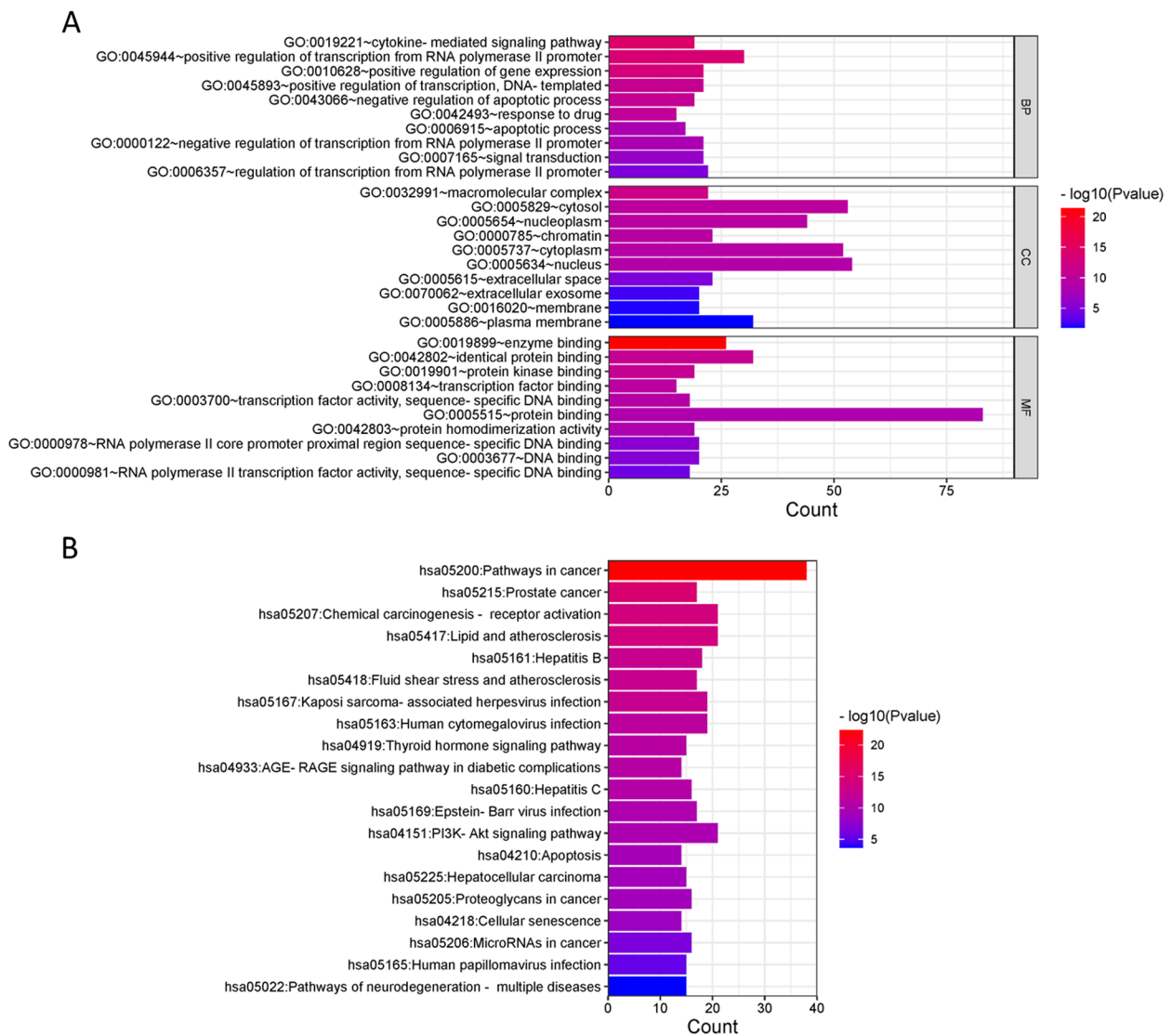
Fig. 3 Results of GO enrichment analysis and KEGG pathway analysis. **A** Horizontal histogram of GO enrichment results. The top graph indicates the results of BP enrichment analysis; the middle graph indicates the results of CC enrichment analysis; the bottom graph indicates the results of MF enrichment analysis. Horizontal coordinates indicate the number of enriched genes. **B** Horizontal histogram of KEGG pathway enrichment results. The Horizontal coordinates indicate the number of enriched genes

Table 1 Molecular docking binding energy of key target proteins and their related active ingredients (kcal/mol)

| Gene	quercetin	luteolin	tanshinone iia	beta-sitosterol	cryptotanshinone
AKT1	-7.8	-6.3	-9.6	-9.7	-9.6
TP53	-10	-7.5	-11.7	-9.8	-11.8
MYC	-7.6	-6	-10	-9.3	-9.9
ESR1	-9.1	-7.4	-11.5	-11.7	-11.5
CASP3	-8.2	-7	-10	-9.9	-10
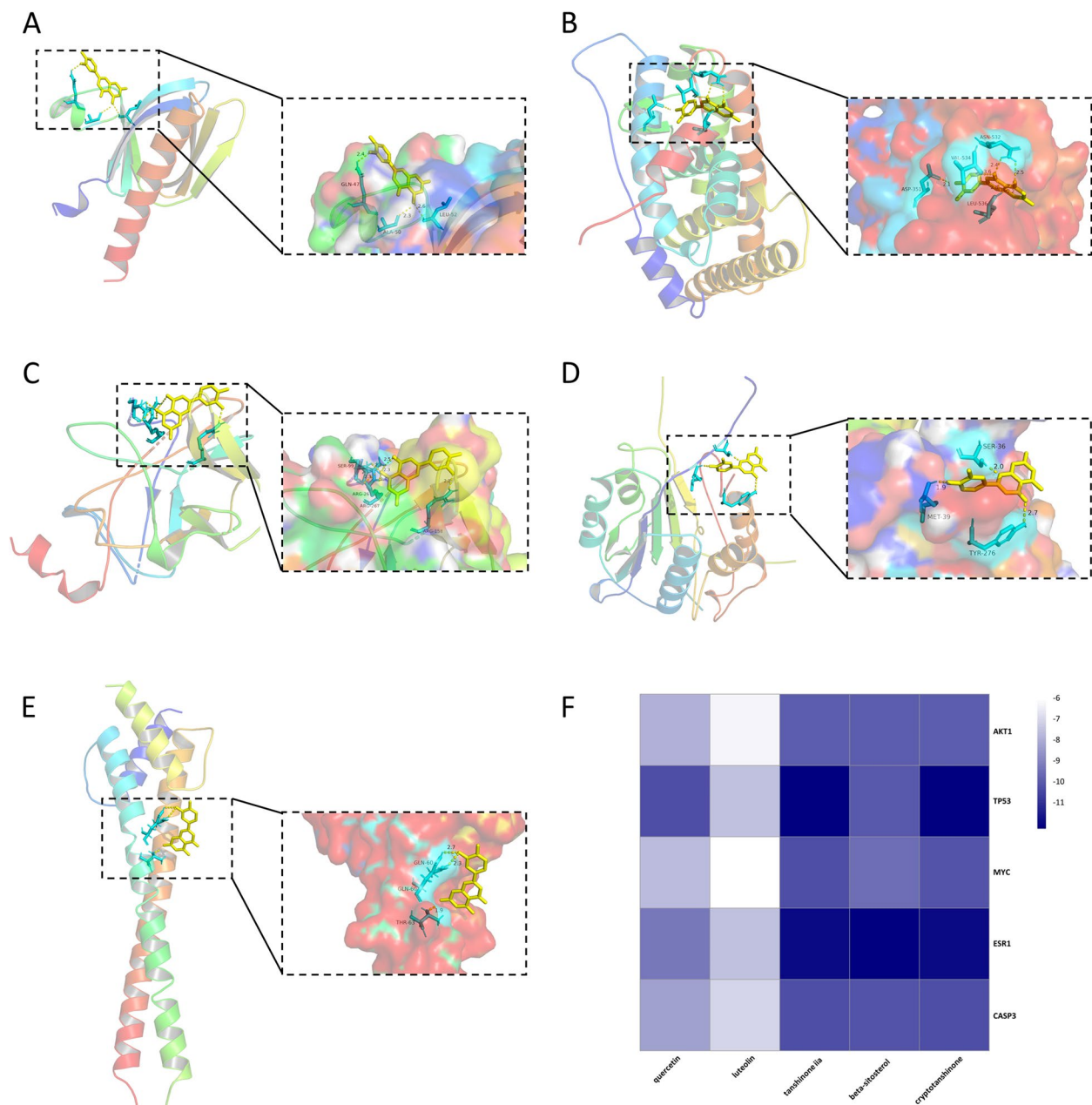
Fig. 4 Molecular docking results of key targets and active ingredients. **A** Molecular docking pattern of luteolin and AKT1. **B** Molecular docking pattern of luteolin and ESR1. **C** Molecular docking pattern of luteolin and TP53. **D** Molecular docking pattern of luteolin and CASP3. **E** Molecular docking pattern of luteolin and MYC. **F** Heat map of docking binding energy of key target proteins and corresponding active ingredients

Luteolin inhibits PA-induced activation of PI3K-AKT signaling pathway in HepG2 cells

The orange-red lipid droplets were significantly increased in the PA group compared with the NC group. When 20 mM luteolin was added to the fatty liver model cells, the orange-red lipid droplets in the cells were significantly reduced (Fig. 6A). Compared with the NC group, the expression of p-PI3K ($P < 0.05$) and p-AKT ($P < 0.01$) was upregulated, and the p-PI3K/PI3K and p-AKT/AKT ratios were increased ($P < 0.05$) in the PA group (Fig. 6B, C, F, E, H). p-PI3K ($P < 0.05$) and p-AKT ($P < 0.01$) were downregulated in the PA+luteolin group compared with the PA group, and p-PI3K/PI3K and p-AKT/AKT ratios were decreased ($P < 0.05$) (Fig. 6B, C, F, E, H). There was no significant difference in PI3K and AKT protein expression levels among the three groups ($P > 0.05$) (Fig. 6D, G).

Chen *et al. BMC Complementary Medicine and Therapies*   (2024) 24:305

Page 9 of 17
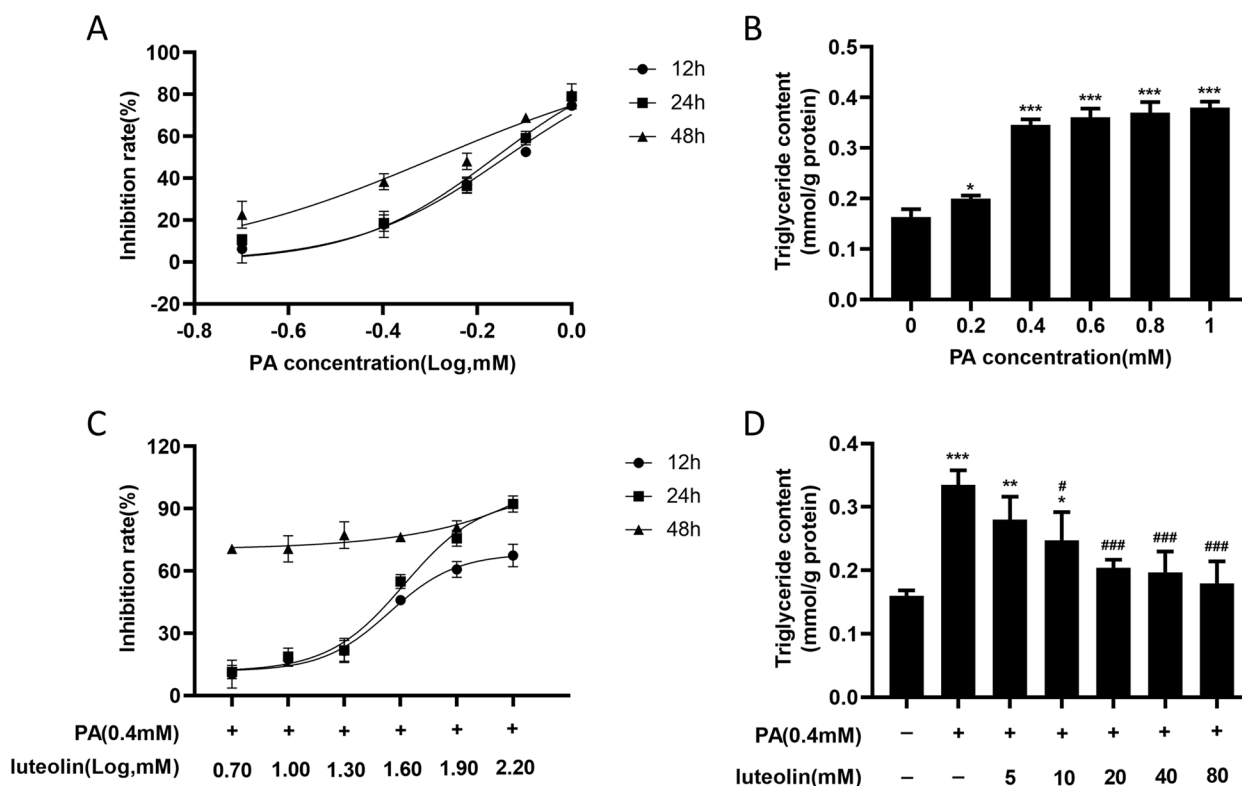
Fig. 5 Effects of PA and luteolin on activity and triglyceride content in HepG2 cells. $n = 3$, $*P < 0.05$, $**P < 0.01$, $***P < 0.001$, vs the control group; $\#P < 0.05$, $\#\#\#P < 0.001$, vs the PA group. **A** Inhibition rate curves of HepG2 cells induced by different time concentrations of PA. **B** Intracellular triglyceride content of HepG2 cells induced by different concentrations of PA. **C** Effect of different time concentrations of luteolin on the inhibition rate curves of HepG2 cells induced by PA. **D** Effect of different concentrations of luteolin on the intracellular triglyceride content of HepG2 cells induced by PA

Effect of luteolin on PA-induced expression of mTOR signaling pathway and autophagy-related proteins in HepG2 cells

Compared with the NC group, the expression of p-mTOR ($P < 0.01$) and p62 ($P < 0.05$) was upregulated, LC3B expression was downregulated ($P < 0.05$) and the p-mTOR/mTOR ratio was increased ($P < 0.001$) in the PA group (Fig. 7A, B, D, E, F). p-mTOR ($P < 0.01$) and p62 ($P < 0.05$) expression in the PA + luteolin group were higher than those in the PA group, LC3B expression was upregulated ($P < 0.05$) and p-mTOR/mTOR ratio was decreased ($P < 0.001$) compared with the PA group (Fig. 7A, B, D, E, F). There was no significant difference in mTOR protein expression levels among the three groups (Fig. 7A, C).

SC79 reverses the effect of luteolin on PI3K-AKT signaling pathway in PA-induced HepG2 cells

Under the condition of 0.4 mM PA and 20 mM luteolin, the cell inhibition rate curve was plotted (Fig. 8A). The IC50 value of SC79 intervention on the inhibition rate of HepG2 cells was calculated by regression equation as 6.473 μM. The intervention concentration of SC79 was formulated as 5 μM.

The p-AKT ($P < 0.01$) and p-PI3K ($P < 0.001$) protein expression, p-PI3K/PI3K ($P < 0.001$) and p-AKT/AKT ($P < 0.001$) ratios were upregulated in the PA group compared with the NC group. After adding luteolin, the p-AKT and p-PI3K proteins, p-PI3K/PI3K and p-AKT/AKT ratios were downregulated compared to the PA group ($P < 0.001$). After the addition of SC79, p-AKT ($P < 0.05$) and p-PI3K ($P < 0.01$) protein expression, p-PI3K/PI3K ($P < 0.05$) and p-AKT/AKT ($P < 0.05$) ratios were upregulated compared to the PA + luteolin group and downregulated compared to the PA + SC79 group. The p-AKT and p-PI3K protein expression, p-PI3K/PI3K and p-AKT/AKT ratios were upregulated in the PA + SC79 group compared with the rest of the groups. The AKT and PI3K protein expression levels were not significantly different in each group (Fig. 8B-H).

SC79 reverses the effects of luteolin on mTOR signaling pathway and autophagy-related protein expression in PA-induced HepG2 cells

The p-mTOR ($P < 0.05$) and p62 ($P < 0.01$) protein expression and p-mTOR/ mTOR ($P < 0.05$) ratio were upregulated in the PA group compared with the NC group, and the LC3B protein expression level was downregulated
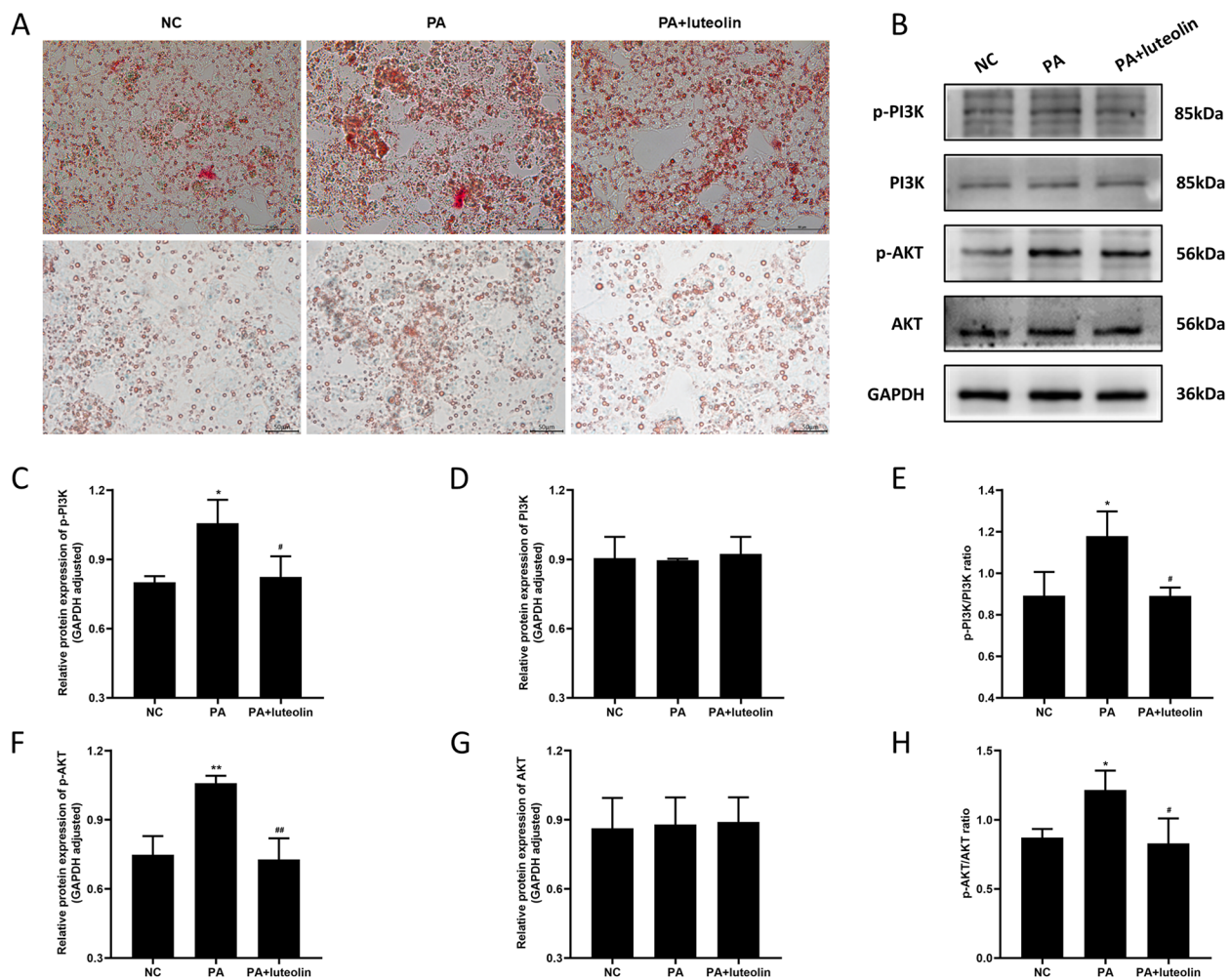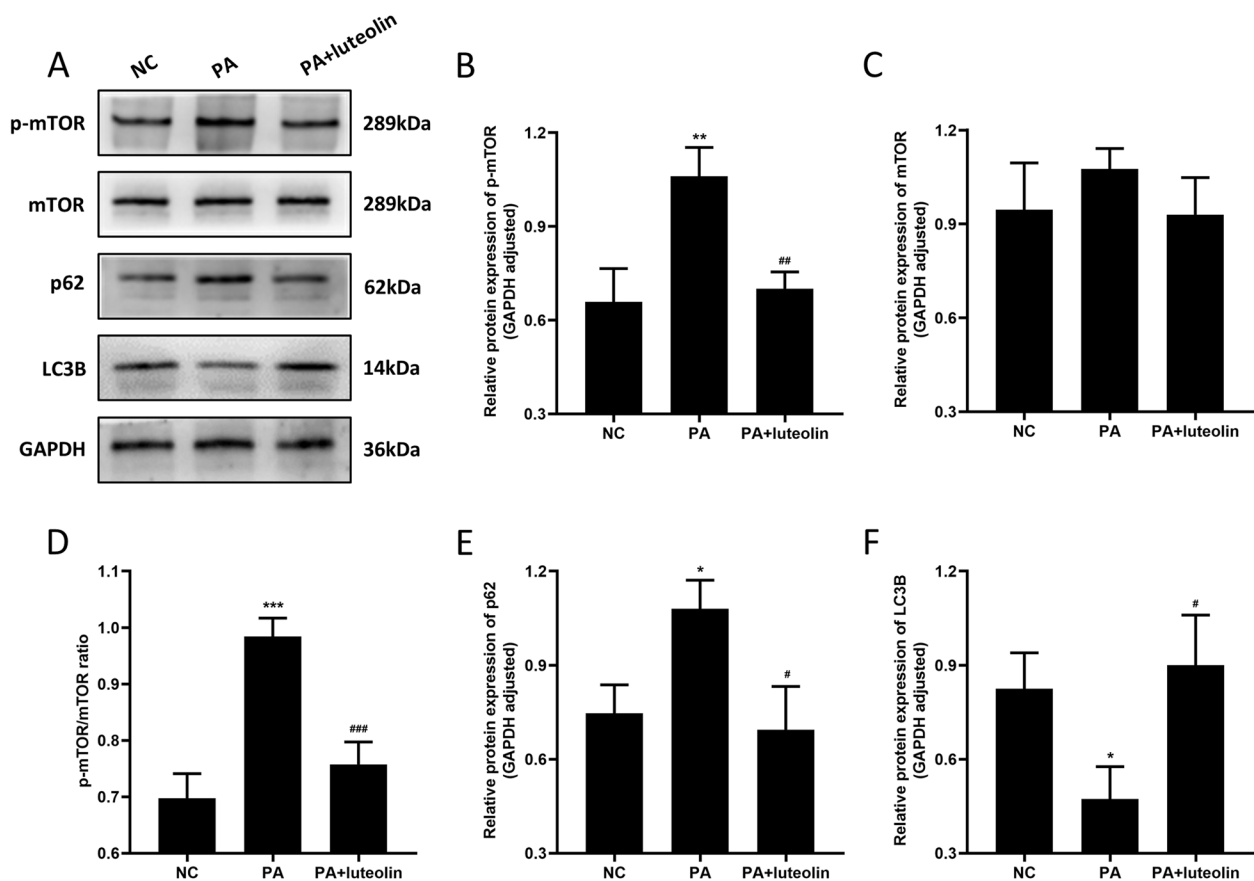
Fig. 6 Luteolin inhibits the activation of PI3K-AKT signaling pathway in PA-induced HepG2 fatty liver cells. $n = 3$, *$P < 0.05$, **$P < 0.01$, vs the control group; #$P < 0.05$, ##$P < 0.01$, vs the PA group. **A** Oil red O staining to observe the effect of luteolin intervention on PA-induced lipid deposition in HepG2 cells. **B** Western blot assay to detect the effect of luteolin on p-PI3K, PI3K, p-AKT, AKT expression in PA-induced HepG2 cells. **C-D** Gray-scale value analysis of the effect of luteolin on p-PI3K and PI3K expression in PA-induced HepG2 cell. **E** Effect of luteolin on p-PI3K/PI3K ratio in PA-induced HepG2 cells. **F-G** Gray-scale value analysis of the effect of luteolin on p-AKT and AKT expression in PA-induced HepG2 cells. **H** Effect of luteolin on p-AKT/AKT ratio in PA-induced HepG2 cells

($P < 0.05$). After the addition of luteolin, p-mTOR ($P < 0.01$), p62 ($P < 0.05$) protein expression and p-mTOR/mTOR ($P < 0.05$) ratio was downregulated and LC3B protein expression level was upregulated compared to the PA group ($P < 0.05$). After adding SC79 again, p-mTOR ($P < 0.01$), p62 ($P < 0.05$) protein expression and p-mTOR/mTOR ($P < 0.05$) ratio were upregulated compared to the PA + luteolin group. After adding SC79 again, LC3B protein expression level was downregulated ($P < 0.01$) compared to PA + luteolin group and upregulated ($P < 0.001$) compared to PA + SC79 group. p-mTOR, p62 protein expression and p-mTOR/mTOR ratio were upregulated and LC3B protein expression was down-regulated in PA + SC79 group compared with the rest of the groups (Fig. 9A-F).

Oil red O staining showed that the orange-red lipid droplets in the cells of PA group were significantly increased compared with NC group. The orange-red lipid droplets in the cells of PA + luteolin group were decreased compared with PA group and the orange-red lipid droplets in the cells of PA + luteolin + SC79 group were increased again (Fig. 9G).

Discussion

In this study, considering the complexity of the active metabolites in SRDP and the diversity of potential human regulatory targets, we collected the targets of SRDP and NAFLD from multiple databases through network analysis to identify common interaction targets. Then, a drug-active metabolite-target-disease network diagram was

Fig. 7 Effects of luteolin on mTOR signaling pathway and autophagy-related protein expression in PA-induced HepG2 fatty liver cells. $n = 3$, *$P < 0.05$, **$P < 0.01$, ***$P < 0.001$, vs the control group; #$P < 0.05$, ##$P < 0.01$, ###$P < 0.001$, vs the PA group. **A** Western blot assay for the effect of luteolin on PA-induced p-mTOR, mTOR, p62, LC3B expression in HepG2 cells. **B-C** Gray-scale value analysis of the effect of luteolin on p-mTOR and mTOR expression in PA-induced HepG2 cells. **D** Effect of luteolin on p-mTOR/mTOR ratio in PA-induced HepG2 cells. **E**–**F** Gray-scale value analysis of the effect of luteolin on p62 and LC3B expression in PA-induced HepG2 cells

constructed. Based on the potential target genes, GO and KEGG enrichment analysis were conducted to predict the potential therapeutic mechanism of SRDP for NAFLD.

We observed that SRDP may exert its therapeutic effects on NAFLD through major active metabolites such as quercetin, luteolin, tanshinone IIA, β-sitosterol, and cryptotanshinone. All of the above active metabolites have been associated with NAFLD treatment. The results of NAFLD and quercetin treatment models established in vivo and in vitro suggest that quercetin could improve AKT phosphorylation, oxidative stress, inflammation and lipid metabolism in liver [22, 23]. Quercetin was found to activate farnesin X receptor 1/Takeda G protein-coupled receptor 5 signaling in addition to significantly attenuating interleukin 1β, interleukin 6, and TNF-α production in NAFLD pathway, which may be one of the ways in which it exerts its therapeutic effects in NAFLD [23]. Similar results

were obtained in clinical studies [24]. In NAFLD cell model experiments, tanshinone IIA attenuated lipid droplet accumulation and down-regulated the expression of lipogenic gene by regulating the LXRα/SREBP1 pathway in hepatocytes. It also reduced cellular inflammation to mitigate fatty liver progression by inhibiting tumor necrosis factor (TNF), transforming growth factor β1 (TGFB1), and interleukin 1β (IL1B) expression [25]. Animal experimental studies demonstrated that tanshinone IIA improved oxidative stress, inflammation, and apoptosis in the liver of rats with hepatic steatosis, regulated cholesterol uptake and efflux, and corrected lipid metabolism disorders [26]. β-sitosterol is the most common type of phytosterol (PS), which can competitively inhibit intestinal cholesterol absorption and slow down the occurrence of hyperlipidemia. It also has various activities such as antioxidant, hypoglycemic, and anti-inflammatory [27]. Experimental and clinical studies have confirmed that β-sitosterol
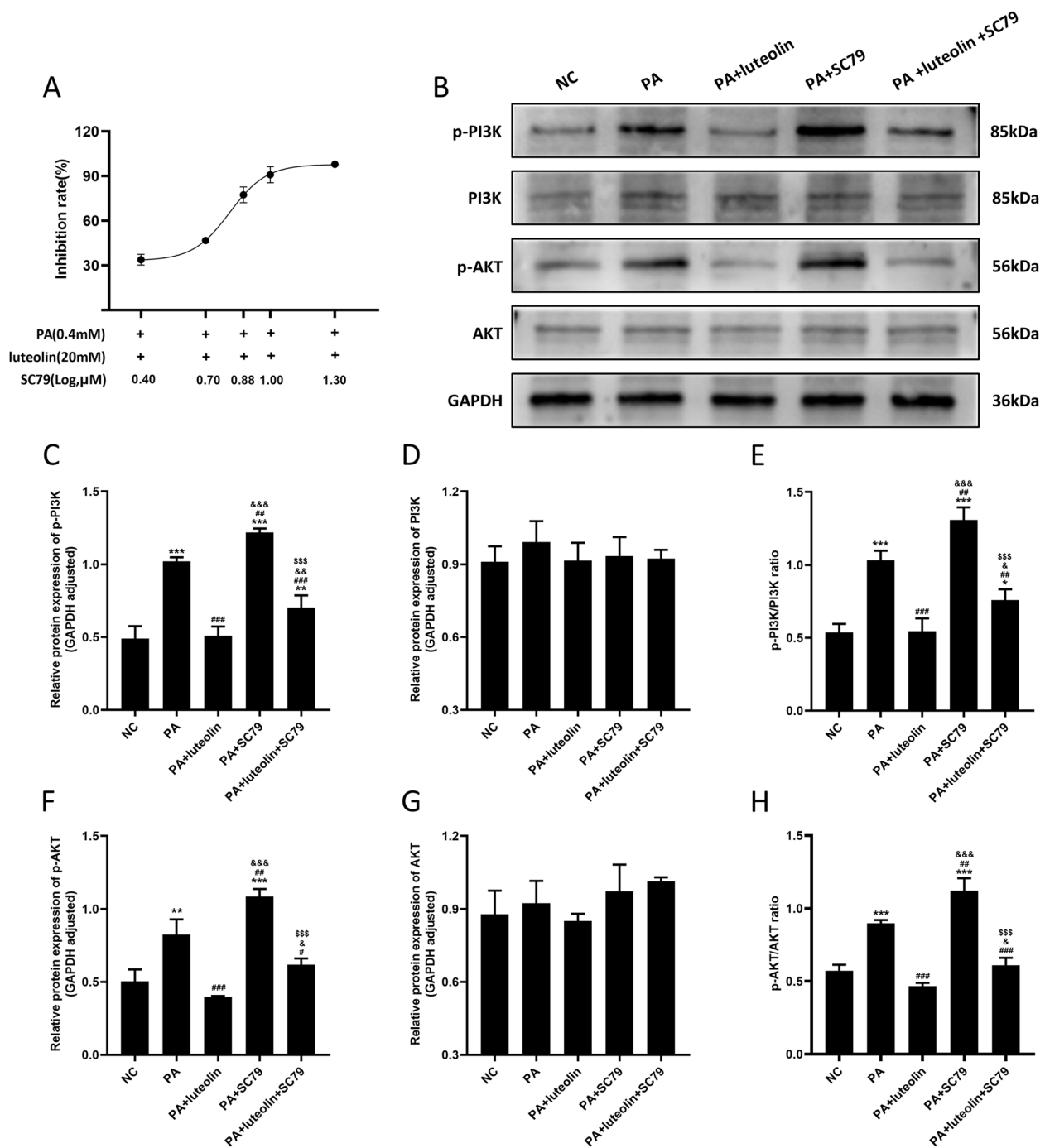
Fig. 8 SC79 reverses the effect of luteolin on PI3K-AKT signaling pathway in PA-induced HepG2 cells. $n = 3$, *$P < 0.05$, **$P < 0.01$, ***$P < 0.001$, vs the control group; #$P < 0.05$, ##$P < 0.01$, ###$P < 0.001$, vs the PA group; &$P < 0.05$, &&$P < 0.01$, &&&$P < 0.001$, vs the PA + luteolin group; $$$$P < 0.001$, vs the PA + SC79 group. **A** Effect of different concentrations of SC79 on the inhibition rate curve of HepG2 cells induced by PA + luteolin. **B** Western blot method to detect the expression of p-PI3K, PI3K, p-AKT in HepG2 cells in NC group, PA group, PA + luteolin group, PA + SC79 group and PA + luteolin + SC79 group. **C-D** Gray-scale value analysis of p-PI3K and PI3K expression in HepG2 cells. **E** The p-PI3K/PI3K ratio in HepG2 cells. **F-G** Gray-scale value analysis of p-AKT and AKT expression in HepG2 cells. **H** The p-AKT/AKT ratio in HepG2 cells
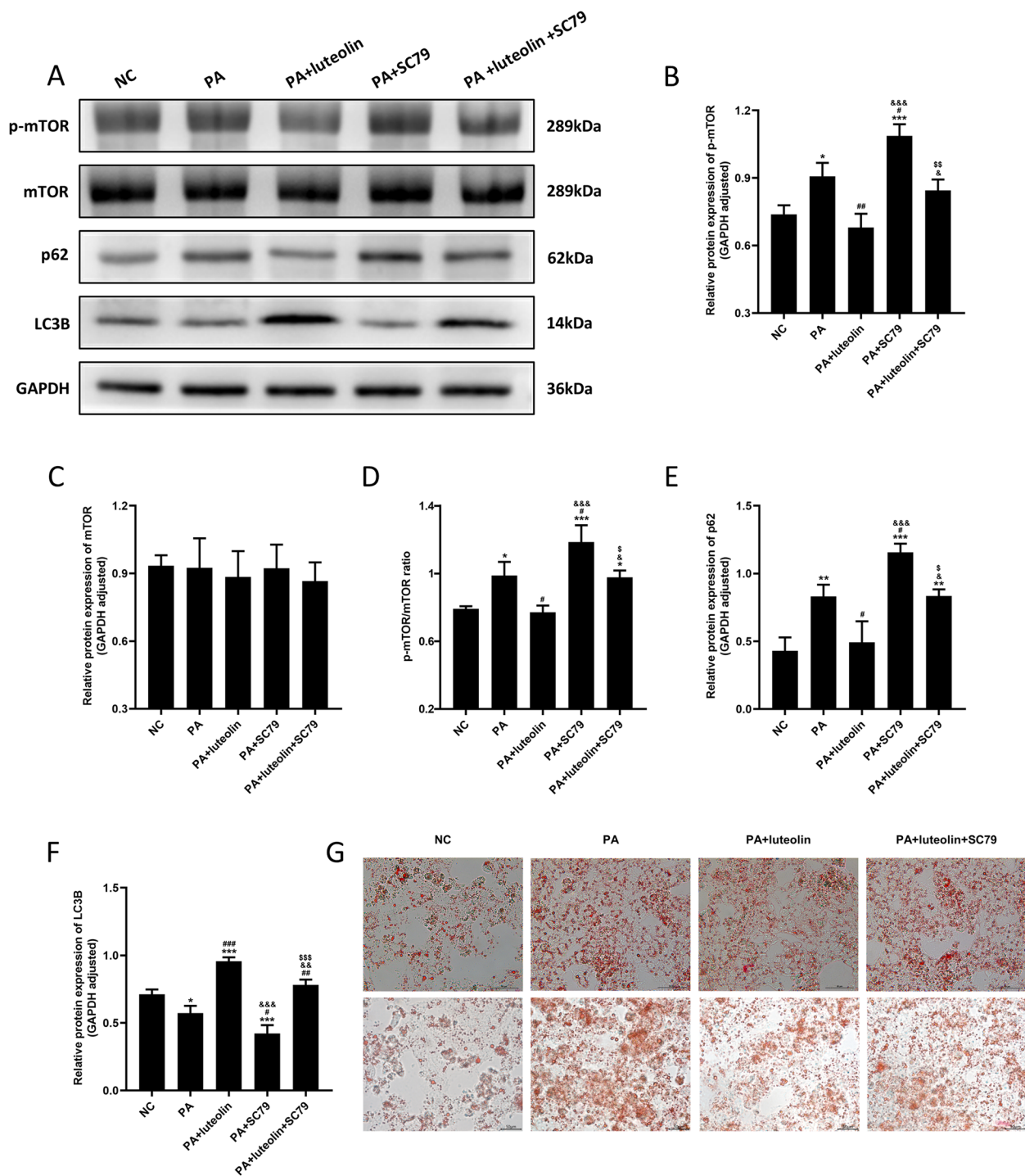
Fig. 9 SC79 reverses the effect of luteolin on mTOR signaling pathway and autophagy-related protein expression in PA-induced HepG2 cells. $n = 3$, $*P < 0.05$, $**P < 0.01$, $***P < 0.001$, vs the control group; $\#P < 0.05$, $\#\#P < 0.01$, $\#\#\#P < 0.001$, vs the PA group; $\&P < 0.05$, $\&\&P < 0.01$, $\&\&\&P < 0.001$, vs the PA + luteolin group; $\$P < 0.05$, $\$\$P < 0.01$, $\$\$\$P < 0.001$, vs the PA + SC79 group. **A** Western blot method to detect the expression of p-mTOR, mTOR, p62, LC3B in HepG2 cells of NC group, PA group, PA + luteolin group, PA + SC79 group and PA + luteolin + SC79 group. **B**-**C** Gray-scale value analysis of p-mTOR and mTOR expression in HepG2 cells. **D** The p-mTOR/ mTOR ratio in HepG2 cells. **E**–**F** Gray-scale value analysis of p62 and LC3B expression in HepG2 cells. **G** Observation of the effect of lipid deposition in HepG2 cells by oil red O staining

can effectively reduce cholesterol and transaminases in NAFLD, improve insulin resistance in NAFLD patients, inhibit systemic inflammation, and enhance antioxidant capacity [28, 29]. Cryptotanshinone blocked calcium 2 + signaling and induction of mitochondrial reactive oxygen species (mtROS) and inhibited NLRP3 inflammatory vesicle activation in a mouse model of NASH [30].

The core active metabolite, luteolin, is abundantly found in vegetables, fruits, and natural botanical drugs, which has significant antioxidant, anti-inflammatory, and metabolic function modulating activities. Its therapeutic role in NAFLD is continuously being explored. It activates heme oxygenase-1 (HO1)-based anti-inflammatory and antioxidant activity by inhibiting nuclear factor -κB (NF-κB) [31]. It can also treat inflammatory activity by inhibiting COX-2, interleukin, and TNF. In addition, luteolin inhibits the production of inducible nitric oxide (iNO) and pro-inflammatory cytokines to exert anti-inflammatory effects [32]. Through acting on the hypothalamus, liver, adipose tissue, and other organs, luteolin can improve lipid and glucose metabolism by the body circulation [33]. Luteolin remarkably down-regulates the expression of gluconeogenesis and lipogenesis genes, reduces liver glucose production, and liver steatosis [34]. Luteolin has been found to enhance the synthesis of serotonin in ADF neurons and activate serotonin receptors MOD-1 and SER-6, thus inducing lipolysis and fatty acid β -oxidation [35]. Another study also demonstrated that luteolin increased glucose utilization, decreased hepatic glucose output, improved systemic and hepatic insulin sensitivity, corrected insulin secretion disorders, and enhanced insulin sensitivity [36]. In this study, we also found that luteolin significantly relieved lipid deposition in PA-induced HepG2 fatty liver cells, consistent with the results of above studies. The above evidence suggests that the active metabolites of SRDP may improve NAFLD by reducing oxidative stress, decreasing lipid accumulation, anti-lipid degeneration, and anti-inflammation.

The most highly interacting targets in the PPI network includes AKT1, TP53, MYC, ESR1, and CASP3, which are more likely to produce cascading effects on NAFLD. AKT1 is a member of the AKT kinase family, which regulates glycolipid metabolism, proliferation and cell survival through a series of downstream substrates. Injection of AKT plasmid via the tail vein in mice can accelerate liver steatosis and inflammatory damage, and a non-alcoholic fatty liver model with gradually aggravating lesions can be formed over three weeks [37]. Activation and amplification of AKT signal transduction accelerated the development of NAFLD in mice. Treatment with AKT

inhibitors improved the development process of NAFLD [38]. Meanwhile, molecular docking results showed that the key active ingredients of DHHP, including quercetin, luteolin, tanshinone II A, β-sitosterol, and cryptotanshinone, exhibited strong binding activities with the core targets of AKT1, TP53, MYC, ESR1, and CASP3. We hypothesize that SRDP can delay the progression of NAFLD through key targets, such as AKT1.

GO enrichment analysis revealed that active metabolites of SRDP tend to regulate DNA transcription by activating transcription-related factors, as the treatment for NAFLD. Besides, they regulate the translation and modification processes to produce functional proteins that participate in the processes of glycolipid metabolism, oxidative stress, inflammation, cell proliferation and apoptosis, thereby reducing liver lipid accumulation. The KEGG pathway analysis provided new insights into the molecular mechanisms of SRDP in treating NAFLD. In order of the number of enriched genes, the pathways most closely related to NAFLD are PI3K-AKT, AGE-RAGE, MAPK, HIF-1, and p53 signaling pathway. The PI3K-AKT pathway is the most interesting one, which plays an important regulatory role in the occurrence and development of NAFLD. Based on the above analysis, it is known that luteolin has a significant ameliorative effect on metabolic diseases. Therefore, in this study, we selected luteolin, the main active metabolite of SRDP, to conduct experimental verification on the effect of this pathway. Based on the previous research results [39] and literature review, the autophagy pathway plays an important role in regulating cellular lipid metabolism. In this study, in vitro cellular experiments confirmed that luteolin could regulate the mTOR pathway through PI3K-AKT signaling pathway and enhance autophagy to alleviate NAFLD.

This study found that the alleviation of NAFLD by luteolin is related to PI3K-AKT signaling pathway, which serves as a crucial pathway for glucolipid metabolism. After insulin specifically binding to insulin receptor on the surface of hepatocytes, IRS is phosphorylated. IRS recruits p85 regulatory subunit of downstream PI3K through SH2 domain to promote PI3K phosphorylation and catalyze the conversion of phosphatidylinositol 4, 5- bisphosphate (PIP2) into phosphatidylinositol 3, 4, 5- trisphosphate (PIP3). PIP3 is the main mediator that mediates the insulin PI3K-dependent biological effects. PIP3 combines with the PH domain of AKT to promote its activation, which plays an important role in the occurrence and development of NAFLD by regulating different targets and pathways such as downstream GSK-3, FOXO pathway, and mTOR [40, 41]. The results of this study showed that luteolin inhibited the phosphorylation of

PI3K-AKT pathway and alleviated the PA-induced lipid deposition in HepG2 NAFLD model. And this alleviation can be reversed by AKT phosphorylation activator SC79. We further found that luteolin, by regulating the PI3K-AKT pathway, inhibited the mTOR pathway and restored autophagy, thereby improving NAFLD.

mTOR is recognized as a central node in the regulatory network for cell growth and development, closely related to hepatic lipid metabolism and other processes. It is involved in regulating lipid metabolism, insulin resistance, oxidative stress, inflammation, autophagy, and other aspects of NAFLD [42]. As a classical downstream effector molecule of the PI3K-AKT pathway, mTOR is an important target for regulating cell growth, proliferation and autophagy. mTOR activity is the key to autophagosome formation and maturation [43]. PI3Ks were divided into three types. When PI3K type I was activated, the AKT-mTOR signaling pathway was activated to inhibit cell autophagy. When PI3K type III was activated, beclin-1 was activated to initiate the autophagy process [44]. Autophagosome formation degrades misfolded proteins and senescent organelles, promotes normal cell growth and development. Hepatic autophagy contributes to essential liver functions including glycogenolysis, gluconeogenesis, and β-oxidation through selective turnover of specific cargoes controlled by a series of transcription factors [45]. Within certain limits, upregulation of autophagy levels can effectively reduce lipid deposition in hepatocytes, so the search for natural/chemical compounds and drugs of the autophagic pathway has become an important avenue for the treatment of NAFLD [45, 46]. mTOR is present in two complexes involved in the control of related signaling pathways: mTORC1 and mTORC2. It is believed that mTORC1 plays a more important role than mTORC2 [42]. When mTORC2 expression is suppressed in mice, activated AKT increases mTORC1 activity and inhibits autophagy by affecting TSC2-Rheb [47, 48]. mTORC2 inhibits Foxo1/3 activity by decreasing AKT activity, which reduces autophagy protein production and inhibits autophagy induction [49]. Both mTORC1 and mTORC2 play important roles in autophagy, and there is an interaction between mTOR and AKT. It is expected that mTOR will be a target for autophagy intervention in the treatment of liver disease.

This study was based on database information for network analysis and in vitro experiments. Yet network analysis is based on database and analysis software, but due to the current technical level, the database is not perfect, and the data in it may be incomplete or noisy. The metabolic network of botanical drug of Chinese medicine is very complex, and it is difficult to fully simulate this complexity in network analysis.

Conclusion

In summary, this study analyzed and predicted the potential mechanism of SRDP on NAFLD through network analysis and molecular docking verification. The results suggested that multiple active metabolites in SRDP may play a role in the treatment of NAFLD through multiple targets and signaling pathways. In vitro cellular assays confirmed that luteolin, the main active metabolite of SRDP, can act on PI3K-AKT-mTOR signaling pathway to induce autophagy, leading to alleviate NAFLD.

Supplementary Information

The online version contains supplementary material available at https://doi.org/10.1186/s12906-024-04600-4.

Supplementary Material 1

Declarations

Competing interests

The authors declare no competing interests.

Author details

[1]Department of Endocrinology and Metabolism, the Second School of Clinical Medicine, Zhujiang Hospital, Southern Medical University, Guangzhou, Guangdong, China. [2]Department of Endocrinology and Metabolism, Shunde Hospital, Southern Medical University (The First People's Hospital of Shunde, Foshan), Foshan, Guangdong, China. [3]Department of Nutrition, the Second School of Clinical Medicine, Zhujiang Hospital, Southern Medical University, Guangzhou, Guangdong, China. [4]Department of Nutrition and Food Hygiene, Guangdong Provincial Key Laboratory of Tropical Disease Research, School of Public Health, Southern Medical University, Guangzhou, Guangdong, China.

References

1. Mazhar K. The Future of Nonalcoholic Fatty Liver Disease Treatment. Med Clin North Am. 2019;103(1):57–69.
2. Singh S, Allen AM, Wang Z, Prokop LJ, Murad MH, Loomba R. Fibrosis progression in nonalcoholic fatty liver vs nonalcoholic steatohepatitis:

a systematic review and meta-analysis of paired-biopsy studies. Clin Gastroenterol Hepatol. 2015;13(4):643–54 e641–649; quiz e639–640.

3. Raza S, Rajak S, Upadhyay A, Tewari A, Anthony SR. Current treatment paradigms and emerging therapies for NAFLD/NASH. Front Biosci (Landmark Ed). 2021;26(2):206–37.

4. Chen M, Xie Y, Gong S, Wang Y, Yu H, Zhou T, Huang F, Guo X, Zhang H, Huang R, Han Z, Xing Y, Liu Q, Tong G, Zhou H. Traditional Chinese medicine in the treatment of nonalcoholic steatohepatitis. Pharmacol Res. 2021;172: 105849.

5. Tan Y, Kamal MA, Wang ZZ, Xiao W, Seale JP, Qu X. Chinese herbal extracts (SK0506) as a potential candidate for the therapy of the metabolic syndrome. Clin Sci (Lond). 2011;120(7):297–305.

6. Liu J, Shi Y, Peng D, Wang L, Yu N, Wang G, Chen W. Salvia miltiorrhiza Bge. (Danshen) in the Treating Non-alcoholic Fatty Liver Disease Based on the Regulator of Metabolic Targets. Front Cardiovasc Med. 2022;9:842980.

7. Peng H, He Y, Zheng G, Zhang W, Yao Z, Xie W. Meta-analysis of traditional herbal medicine in the treatment of nonalcoholic fatty liver disease. Cell Mol Biol (Noisy-le-grand). 2016;62(4):88–95.

8. Wang W, Xu AL, Li ZC, Li Y, Xu SF, Sang HC, Zhi F. Combination of Probiotics and Salvia miltiorrhiza Polysaccharide Alleviates Hepatic Steatosis via Gut Microbiota Modulation and Insulin Resistance Improvement in High Fat-Induced NAFLD Mice. Diabetes Metab J. 2020;44(2):336–48.

9. Fan HT, Ding SL, Lin HS. Pharmacological of Polygoni cuspidati rhizoma. Zhongguo Zhong Yao Za Zhi. 2013;38(15):2545–8.

10. Huang Y, Lang H, Chen K, Zhang Y, Gao Y, Ran L, Yi L, Mi M, Zhang Q. Resveratrol protects against nonalcoholic fatty liver disease by improving lipid metabolism and redox homeostasis via the PPARα pathway. Appl Physiol Nutr Metab. 2020;45(3):227–39.

11. Hubbard BP, Sinclair DA. Small molecule SIRT1 activators for the treatment of aging and age-related diseases. Trends Pharmacol Sci. 2014;35(3):146–54.

12. Kim J, Kim CS, Jo K, Lee IS, Kim JH, Kim JS. POCU1b, the n-Butanol Soluble Fraction of Polygoni Cuspidati Rhizoma et Radix, Attenuates Obesity, Non-Alcoholic Fatty Liver, and Insulin Resistance via Inhibitions of Pancreatic Lipase, cAMP-Dependent PDE Activity, AMPK Activation, and SOCS-3 Suppression. Nutrients. 2020;12(12):3612.

13. Yu ZG. Observation of curative effect on Shuanghu Qinggan Particles combined with Dantian Jiangzhi Wan in the treatment of fatty liver hepatitis. China Modern Medicine. 2012;19(05):110–1.

14. Qi FH, Wang ZX, Cai PP, Zhao L, Gao JJ, Kokudo N, Li AY, Han JQ, Tang W. Traditional Chinese medicine and related active compounds: a review of their role on hepatitis B virus infection. Drug Discov Ther. 2013;7(6):212–24.

15. Ru J, Li P, Wang J, Zhou W, Li B, Huang C, Li P, Guo Z, Tao W, Yang Y, Xu X, Li Y, Wang Y, Yang L. TCMSP: a database of systems pharmacology for drug discovery from herbal medicines. J Cheminform. 2014;6:13.

16. UniProt C. UniProt: the universal protein knowledgebase in 2021. Nucleic Acids Res. 2021;49(D1):D480–9.

17. Safran M, Dalah I, Alexander J, Rosen N, Iny ST, Shmoish M, Nativ N, Bahir I, Doniger T, Krug H, Sirota-Madi A, Olender T, Golan Y, Stelzer G, Harel A, Lancet D. GeneCards Version 3: the human gene integrator. Database (Oxford). 2010;2010:baq020.

18. Hamosh A, Scott AF, Amberger JS, Bocchini CA, Mckusick VA. Online Mendelian Inheritance in Man (OMIM), a knowledgebase of human genes and genetic disorders. Nucleic Acids Res. 2005;33(Database issue):D514–517.

19. Shannon P, Markiel A, Ozier O, Baliga NS, Wang JT, Ramage D, Amin N, Schwikowski B, Ideker T. Cytoscape: a software environment for integrated models of biomolecular interaction networks. Genome Res. 2003;13(11):2498–504.

20. Szklarczyk D, Gable AL, Lyon D, Junge A, Wyder S, Huerta-Cepas J, Simonovic M, Doncheva NT, Morris JH, Bork P, Jensen LJ, Mering CV. STRING v11: protein-protein association networks with increased coverage, supporting functional discovery in genome-wide experimental datasets. Nucleic Acids Res. 2019;47(D1):D607–13.

21. Huang DW, Sherman BT, Tan Q, Kir J, Liu D, Bryant D, Guo Y, Stephens R, Baseler MW, Lane HC, Lempicki RA. DAVID Bioinformatics Resources: expanded annotation database and novel algorithms to better extract biology from large gene lists. Nucleic Acids Res. 2007;35(Web Server issue):W169–175.

22. Pisonero-Vaquero S, Martínez-Ferreras Á, García-Mediavilla MV, Martínez-Flórez S, Fernández A, Benet M, Olcoz JL, Jover R, González-Gallego J, Sánchez-Campos S. Quercetin ameliorates dysregulation of lipid metabolism genes via the PI3K/AKT pathway in a diet-induced mouse model of nonalcoholic fatty liver disease. Mol Nutr Food Res. 2015;59(5):879–93.

23. Yang H, Yang T, Heng C, Zhou Y, Jiang Z, Qian X, Du L, Mao S, Yin X, Lu Q. Quercetin improves nonalcoholic fatty liver by ameliorating inflammation, oxidative stress, and lipid metabolism in db/db mice. Phytother Res. 2019;33(12):3140–52.

24. Prysyazhnyuk VP, Voloshyn OI. Effects of comprehensive treatment with quercetin administration on biochemical blood parameters and pro-and anti-inflammatory cytokines in nonalcoholic fatty liver disease patients. 2017.

25. Gao WY, Chen PY, Hsu HJ, Lin CY, Wu MJ, Yen JH. Tanshinone IIA Downregulates Lipogenic Gene Expression and Attenuates Lipid Accumulation through the Modulation of LXRα/SREBP1 Pathway in HepG2 Cells. Biomedicines. 2021;9(3):326.

26. Jia LQ, Zhang N, Xu Y, Chen WN, Zhu ML, Song N, Ren L, Cao HM, Wang JY, Yang GL. Tanshinone IIA affects the HDL subfractions distribution not serum lipid levels: Involving in intake and efflux of cholesterol. Arch Biochem Biophys. 2016;592:50–9.

27. Rideout TC, Marinangeli CPF, Harding SV. Triglyceride-Lowering Response to Plant Sterol and Stanol Consumption. J AOAC Int. 2015;98(3):707–15.

28. Chen DL, Huang PH, Chiang CH, Leu HB, Chen JW, Lin SJ. Phytosterols increase circulating endothelial progenitor cells and insulin-like growth factor-1 levels in patients with nonalcoholic fatty liver disease: A randomized crossover study. Journal of Functional Foods. 2015;13:148–57.

29. Feng S, Dai Z, Liu AB, Huang J, Narsipur N, Guo G, Kong B, Reuhl K, Lu W, Luo Z, Yang CS. Intake of stigmasterol and β-sitosterol alters lipid metabolism and alleviates NAFLD in mice fed a high-fat western-style diet. Biochim Biophys Acta Mol Cell Biol Lipids. 2018;1863(10):1274–84.

30. Liu H, Zhan X, Xu G, Wang Z, Li R, Wang Y, Qin Q, Shi W, Hou X, Yang R, Wang J, Xiao X, Bai Z. Cryptotanshinone specifically suppresses NLRP3 inflammasome activation and protects against inflammasome-mediated diseases. Pharmacol Res. 2021;164: 105384.

31. Owumi SE, Lewu DO, Arunsi UO, Oyelere AK. Luteolin attenuates doxorubicin-induced derangements of liver and kidney by reducing oxidative and inflammatory stress to suppress apoptosis. Hum Exp Toxicol. 2021;40(10):1656–72.

32. Ma Q, Jiang J G, Zhang X M, Zhu W. Identification of luteolin 7-O-beta-D-glucuronide from Cirsium japonicum and its anti-inflammatory mechanism. J Funct Foods. 2018;(46-):46.

33. Wang Z, Zeng M, Wang Z, Qin F, Chen J, He Z. Dietary Luteolin: A Narrative Review Focusing on Its Pharmacokinetic Properties and Effects on Glycolipid Metabolism. J Agric Food Chem. 2021;69(5):1441–54.

34. Bumke-Vogt C, Osterhoff MA, Borchert A, Guzman-Perez V, Sarem Z, Birkenfeld AL, Bähr V, Pfeiffer AF. The flavones apigenin and luteolin induce FOXO1 translocation but inhibit gluconeogenic and lipogenic gene expression in human cells. PLoS ONE. 2014;9(8): e104321.

35. Lin Y, Yang N, Bao B, Wang L, Chen J, Liu J. Luteolin reduces fat storage in Caenorhabditis elegans by promoting the central serotonin pathway. Food Funct. 2020;11(1):730–40.

36. Park S, Kim DS, Kang S, Kim HJ. The combination of luteolin and l-theanine improved Alzheimer disease-like symptoms by potentiating hippocampal insulin signaling and decreasing neuroinflammation and norepinephrine degradation in amyloid-β-infused rats. Nutr Res. 2018;60:116–31.

37. Yu ZY, He Y, Luo W, Li L. Establishment of AKT Gene-mediated Non-alcoholic Fatty Liver Models in Mice. Acta Medicinae Universitatis Scientiae et Technologiae Huazhong. 2016;45(02):100–5.

38. Jeong SH, Kim HB, Kim MC, Lee JM, Lee JH, Kim JH, Kim JW, Park WY, Kim SY, Kim JB, Kim H, Kim JM, Choi HS, Lim DS. Hippo-mediated suppression of IRS2/AKT signaling prevents hepatic steatosis and liver cancer. J Clin Invest. 2018;128(3):1010–25.

39. Li L, Li Q, Huang W, Han Y, Tan H, An M, Xiang Q, Zhou R, Yang L, Cheng Y. Dapagliflozin Alleviates Hepatic Steatosis by Restoring Autophagy via the AMPK-mTOR Pathway. Front Pharmacol. 2021;12: 589273.

40. Molinaro A, Becattini B, Mazzoli A, Bleve A, Radici L, Maxvall I, Sopasakis VR, Molinaro A, Bäckhed F, Solinas G. Insulin-Driven PI3K-AKT Signaling in the Hepatocyte Is Mediated by Redundant PI3Kα and PI3Kβ Activities and Is Promoted by RAS. Cell Metab. 2019;29(6):1400–1409.e1405.

41. Saltiel AR. Insulin signaling in health and disease. J Clin Invest. 2021;131(1):e142241.
42. Feng J, Qiu S, Zhou S, Tan Y, Bai Y, Cao H, Guo J, Su Z. mTOR: A Potential New Target in Nonalcoholic Fatty Liver Disease. Int J Mol Sci. 2022;23(16):9196.
43. Chang X, Wang X, Li J, Shang M, Niu S, Zhang W, Li Y, Sun Z, Gan J, Li W, Tang M, Xue Y. Silver nanoparticles induced cytotoxicity in HT22 cells through autophagy and apoptosis via PI3K/AKT/mTOR signaling pathway. Ecotoxicol Environ Saf. 2021;208: 111696.
44. Hill SM, Wrobel L, Rubinsztein DC. Post-translational modifications of Beclin 1 provide multiple strategies for autophagy regulation. Cell Death Differ. 2019;26(4):617–29.
45. Ueno T, Komatsu M. Autophagy in the liver: functions in health and disease. Nat Rev Gastroenterol Hepatol. 2017;14(3):170–84.
46. Flessa CM, Kyrou I, Nasiri-Ansari N, Kaltsas G, Papavassiliou AG, Kassi E, Randeva HS. Endoplasmic Reticulum Stress and Autophagy in the Pathogenesis of Non-alcoholic Fatty Liver Disease (NAFLD): Current Evidence and Perspectives. Curr Obes Rep. 2021;10(2):134–61.
47. Annett S, Moore G, Robson T. FK506 binding proteins and inflammation related signalling pathways; basic biology, current status and future prospects for pharmacological intervention. Pharmacol Ther. 2020;215: 107623.
48. Choi AM, Ryter SW, Levine B. Autophagy in human health and disease. N Engl J Med. 2013;368(7):651–62.
49. Spormann L, Rennert C, Kolbe E, Ott F, Lossius C, Lehmann R, Gebhardt R, Berg T, Matz-Soja M. Cyclopamine and Rapamycin Synergistically Inhibit mTOR Signalling in Mouse Hepatocytes, Revealing an Interaction of Hedgehog and mTor Signalling in the Liver. Cells. 2020;9(8):1817.

Publisher's Note